AIMS Mathematics, 10(10): 24294–24316.
DOI: 10.3934/math.20251077
Received: 08 July 2025
Revised: 22 September 2025
Accepted: 16 October 2025
Published: 23 October 2025

https://www.aimspress.com/journal/Math

Research article

A finite integration method for pricing and hedging path-dependent structured derivatives

Yejin Kim[1], **Wooyeol Jeong**[2,*] **and Sungchul Lee**[2]

[1] EG Asset Pricing Co., Ltd., Seoul 07241, Korea
[2] Department of Mathematics, Yonsei University, Seoul 03722, Korea

* **Correspondence:** Email: mathwy@yonsei.ac.kr; Tel: +821031883333.

Abstract: This study introduces the finite integration method (FIM) as a robust numerical approach for pricing equity-linked notes (ELNs). The FIM extends its application beyond vanilla options, effectively addressing the complexities of continuous boundaries and binary payoffs associated with ELNs. We present a comprehensive framework for ELN pricing, including detailed explanations of product structures and a step-by-step description of the FIM methodology. To assess the performance of the FIM, we conduct a comparative analysis against the implicit FDM. Numerical results demonstrate that the FIM outperforms the FDM in terms of reduced pricing errors and more precise hedge parameters (Greeks). We evaluated both one-dimensional barrier options and two-dimensional binary options. Additionally, we proposed an FIM algorithm for pricing a two-dimensional step-down ELN with a knock-in barrier feature. Monte Carlo simulations(MCS) are used as benchmarks to validate the convergence and accuracy of the FIM. The results confirm that the FIM is a robust and practical method for derivative valuation and risk management. Furthermore, the flexibility of the FIM framework allows it to accommodate various complex payoff structures, making it a valuable tool for pricing structured derivatives.

Keywords: finite integration method; equity-linked notes; path-dependent derivatives; Greeks; numerical methods; hedging
Mathematics Subject Classification: 65C20, 91G20

Abbreviations

ELN	Equity-linked Note
FIM	Finite Integration Method
FDM	Finite Difference Method
MCS	Monte Carlo Simulation
PDE	Partial Differential Equation
QMC	Quasi-Monte Carlo
OSM	Operator Splitting Method

1. Introduction

The foundation of modern option pricing theory was established by Black and Scholes (1973), who introduced a closed-form solution for European options under the assumption of constant volatility and frictionless markets [1]. Their breakthrough provided a theoretical framework that has since become the cornerstone of derivative pricing. However, real-world financial markets exhibit complexities that necessitate further refinements. Merton (1973) extended the Black-Scholes framework by incorporating dividend-paying assets and early exercise features, which laid the groundwork for pricing American-style options and dividend-paying derivatives [2]. Recognizing the need for numerical techniques to handle more complex financial instruments, Cox, Ross, and Rubinstein (1979) introduced the binomial tree model, providing a flexible and computationally feasible approach to option valuation [3]. This model paved the way for a broad range of numerical pricing techniques that followed.

Option pricing has been extensively studied using numerical techniques, with two primary approaches being the finite difference method (FDM) and Monte Carlo simulations (MCS). These methods have been widely employed due to their flexibility and applicability to various derivative pricing problems, including structured notes such as equity-linked notes (ELNs), where accurate valuation and sensitivity analysis are essential for effective hedging.

FDM-based approaches have been extensively refined to enhance both accuracy and efficiency in option pricing. Adaptive FDM, including error estimation and space- and time-adaptive techniques, has been developed to efficiently solve high-dimensional stochastic models such as the Heston–Hull–White partial differential equation (PDE), jump-diffusion models, and American options with early exercise features [4–6]. High-order and explicit FDM has also been modified to improve numerical stability and accuracy, particularly for barrier option pricing, through optimized grid placement and higher-order schemes [7, 8]. In the context of barrier options, various techniques have been proposed to address the challenges posed by continuous and discrete monitoring. For instance, [9] developed an analytic framework for pricing European continuous-installment barrier options, while [10] investigated quadrature-based recombining tree methods for discretely monitored single barrier options. These studies emphasized the importance of accurate numerical handling of barrier activation features, which are also critical in ELN pricing. To further address high-dimensionality challenges, non-uniform and sparse grid optimization strategies have been proposed to enhance computational efficiency and robustness [11, 12]. In addition, hybrid tree-FDM and super-time-stepping techniques have been introduced to accelerate explicit FDMs and alleviate stability constraints under complex stochastic models [13,14]. Alternative schemes such as mimetic and compact FDM have been explored to improve

accuracy and stability, particularly in exotic derivatives pricing [15, 16]. Furthermore, quadrature-based methods have demonstrated improved accuracy in pricing structured derivatives such as autocallable products and barrier options [17, 18]. In the context of ELN, FDM has been effectively applied to one- and two-asset cases, whereas MCS remains the primary approach for three-asset ELN due to dimensionality challenges [19].

Due to its flexibility, MCS is widely used in option pricing, particularly for high-dimensional and path-dependent derivatives. However, MCS methods are often limited by slow convergence and high variance. To address these issues, various variance reduction techniques—including importance sampling, control variates, and quasi-Monte Carlo (QMC) methods—have been developed [20, 21]. In particular, QMC methods offer deterministic sequences that improve convergence and error control over standard MCS [22]. Beyond variance reduction, accelerated Monte Carlo under jump-diffusion dynamics has also been explored; for example, [23] develop an accelerated diffusion Monte Carlo scheme with Poisson jumps and adaptive/stratified sampling, reporting substantial speedups in high-dimensional settings. Additionally, parallelization strategies have been actively pursued to enhance the efficiency of MCS, especially for multi-dimensional Bermudan and American options. Recent approaches leverage parallel computing environments to compute optimal exercise boundaries, classify continuation and exercise regions, and improve scalability and computational performance [24]. Further improvements, such as smoothing techniques and optimized path generation, have also been introduced to effectively handle high-dimensional problems and discontinuities in exotic option pricing [25, 26].

Beyond finite-difference and Monte Carlo methods, alternative schemes include quadrature-based valuation [27], mimetic finite-difference methods that preserve monotonicity and conservation [28], finite-element formulations such as discontinuous Galerkin for stochastic-volatility models [29], and refined tree-based methods for complex barriers and continuous monitoring [30]. In contrast, our FIM computes the one-step risk-neutral expectation analytically by integrating a local quadratic surrogate against the lognormal transition density, thereby avoiding quadrature tuning and implicit time stepping while applying correlation and barrier/early-redemption events at observation dates. This makes FIM a natural fit for multi-asset ELNs with discrete monitoring.

In addition, analytical and fractional models have been explored to capture market phenomena such as memory effects and volatility smiles. The homotopy analysis method has been applied to time-fractional Black-Scholes models, yielding improved convergence properties [31]. Fractional extensions of classical models, including time-fractional Black-Scholes and constant elasticity of variance models, have been introduced to incorporate long-memory behaviors and better reflect empirical option price dynamics [32–34]. Most recently, [35] analyzed a fractional-order Black–Scholes model via a band-equation formulation and established convergence for Laplace-transform, Hilbert-transform, and Monte Carlo solvers, providing comparative numerics for fractional European options.

While these advancements have contributed significantly to the field of option pricing, existing numerical methods still face limitations. FDM rely on structured grids, making them less adaptable to structured derivatives such as ELNs, which often involve continuous monitoring and path-dependent features. MCS, despite their flexibility in handling high-dimensional problems, often suffer from slow convergence and high variance, requiring additional computational techniques to improve efficiency. The need for accurate ELN valuation has been underscored by historical events, such as the significant losses observed during the decline of the Hang Seng China Enterprises Index (HSCEI) in 2016, highlighting the importance of precise pricing and risk management frameworks. Given these

challenges, this study introduces the FIM as an alternative numerical approach, aiming to enhance pricing accuracy for structured derivatives, particularly ELNs.

FIM has been successfully applied in the context of one- and multi-dimensional derivatives, as demonstrated by [36, 37], and shows promise in managing complex payoff structures and continuous boundary conditions. Unlike traditional methods, FIM avoids requiring intensive grid adjustments in handling continuous barriers, offering improved accuracy. This makes FIM particularly well-suited for pricing path-dependent structured products like ELNs, which involve continuous monitoring and complex payoff conditions. This study builds on prior applications of the FIM framework, while situating it within the broader landscape of established numerical methods, including finite difference schemes (e.g., [38]) and MCS (e.g., [39]), which serve as representative references. Specifically, we aim to extend the application of FIM to complex ELN structures and examine its effectiveness relative to these traditional approaches.

The structure of this paper is as follows: Section 2.1 provides a brief overview of ELNs, highlighting their unique payoff structure and key characteristics. Section 2.2 details the step-by-step FIM methodology used in this study. In Section 3, we present numerical experiments comparing the performance of FIM against traditional FDM and MCS, focusing on pricing errors and hedge parameter accuracy. The results confirm FIM's effectiveness as a robust approach for accurate ELN pricing and risk analysis. Finally, Section 4 concludes the study by summarizing key findings and discussing potential future research directions to enhance the application of FIM in financial modeling.

2. Materials and methods

2.1. Overview of equity-linked notes

ELNs are structured financial products that combine debt instruments with embedded options tied to the performance of specific equities or indices. ELNs offer a way for investors to achieve potentially higher returns than conventional fixed-income securities, with payouts based on the performance of the underlying assets. Unlike traditional stock or stock options investments, ELNs allow investors to benefit from equity market movements without directly owning equities. This makes ELNs particularly attractive for those seeking passive exposure to market performance without the associated management burden or margin requirements.

When compared with other investment strategies, ELNs present unique advantages and limitations. For instance, direct stock ownership exposes investors to the full volatility of the stock market, requiring significant time and effort to analyze and select stocks. Alternatively, stock options provide leverage but come with high risk due to their short-term nature. In contrast, ELNs offer structured payouts and typically protect investors from losses as long as certain conditions, such as knock-in barriers, are met. This structure enables ELN investors to achieve superior returns compared to traditional fixed-rate products, offering an attractive alternative to bank interest rates.

Figure 1 illustrates the typical payoff structure of a two-asset step-down ELN, which features a three-year maturity and offers early redemption opportunities every six months. This ELN includes two underlying assets, such as the KOSPI200 index and Samsung stock, with designated strike rates K_j and redemption rates r_j at each early redemption date T_j, a dummy rate d at maturity (a fixed return paid under neutral conditions without early redemption or knock-in), and a knock-in barrier B. The strike rates K_j decrease (or "step-down") at each redemption period, ranging from 90% to 80%,

while the redemption rates r_j increase incrementally from 3% up to 18%. The ELN includes a dummy rate $d = 18\%$ at maturity if no knock-in event occurs and a knock-in barrier of $B = 60\%$. This ELN enables investors to secure returns if the underlying assets meet the specified strike levels by providing a structured payoff that adjusts at each redemption period.

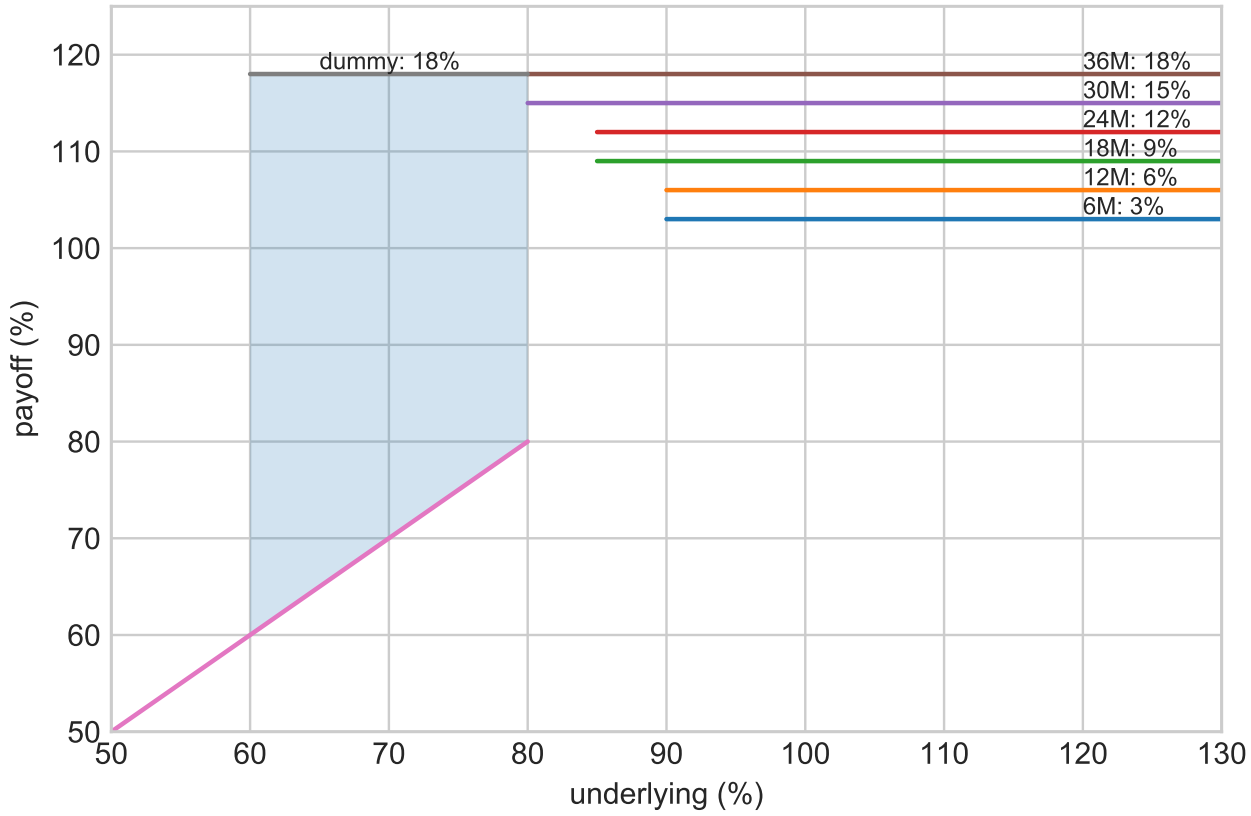

Figure 1. Payoff structure of a step-down ELN with a three-year maturity and semi-annual early redemption opportunities. This figure presents a specific example of a step-down ELN, showcasing its profit and loss structure. It exhibits a decreasing pattern of strike rates, ranging from 90% to 80%, with an annual decrement of 5%. The ELN also features a knock-in barrier set at 60%. The redemption rate is fixed at 6% annually, and the dummy rate at maturity matches the maturity redemption rate at 18%.

The payoff structure of a multi-asset step-down ELN is summarized in Table 1. Below, we provide further details for each case to complement the table:

Case 1: Early Redemption. At each early redemption date T_j, the ELN is subject to early redemption if the minimum return rate of the underlying assets satisfies:

$$\min_i \left(S_i(T_j)/S_i(T_0)\right) \geq K_j.$$

If this condition holds, the investor receives a payoff of $(1 + r_j)N$, where r_j is the predetermined redemption rate, and N is the notional amount. The ELN expires immediately at T_j. For example:

- At T_1, if the condition is met, the investor receives $(1 + r_1)N$.
- The same applies for subsequent dates $T_2, T_3, \ldots, T_{n-1}$.

Table 1. Summary of the payoff structure for a multi-asset step-down ELN with a knock-in barrier. The table outlines the conditions and payoffs for both early redemption (Case 1) and scenarios at maturity (Case 2).

	time	condition	payoff
Case 1	T_1	$\min_i \left(S_i(T_1)/S_i(T_0)\right) \geq K_1$	$(1 + r_1)N$
	T_2	$\min_i \left(S_i(T_2)/S_i(T_0)\right) \geq K_2$	$(1 + r_2)N$
	$\cdots$	$\cdots$	$\cdots$
	T_{n-1}	$\min_i \left(S_i(T_{n-1})/S_i(T_0)\right) \geq K_{n-1}$	$(1 + r_{n-1})N$
Case 2	T_n	$\min_i \left(S_i(T_n)/S_i(T_0)\right) \geq K_n$	$(1 + r_n)N$
	T_n	$\min_{0\leq t\leq T} \min_i \left(S_i(t)/S_i(T_0)\right) \geq B$	$(1 + d)N$
	T_n	$\min_{0\leq t\leq T} \min_i \left(S_i(t)/S_i(T_0)\right) < B$	$\min_i \left(S_i(T_n)/S_i(T_0)\right) N$

Case 2: No Early Redemption. If no early redemption occurs, the ELN continues to maturity T_n. At this point, three possible outcomes arise:

Last Redemption. If

$$\min_i \left(S_i(T_n)/S_i(T_0)\right) \geq K_n,$$

the investor receives $(1 + r_n)N$.

Dummy Payoff. If no underlying asset hits the knock-in barrier during the ELN's lifetime, i.e.,

$$\min_i \left[\min_{0\leq t\leq T} \left(S_i(t)/S_i(T_0)\right)\right] \geq B,$$

the investor receives a dummy payoff of $(1 + d)N$, where d is the predetermined dummy rate.

Knock-in Payoff. If a knock-in event occurs, the investor receives:

$$\min_i [S_i(T_n)/S_i(T_0)]N,$$

which corresponds to the performance of the lowest-performing asset.

Through this structured payout, ELNs exhibit binary and barrier options characteristics, adding layers of complexity that prevent closed-form solutions and make valuation challenging. This complexity highlights the need for accurate numerical methods to assess ELN payoffs and related sensitivities (Greeks) under various scenarios. The FDM and MCS are two commonly used numerical methods for ELN pricing. Each method offers distinct benefits and limitations in terms of accuracy. FDM is widely used for its accuracy and stability in derivatives pricing, particularly when handling multi-asset and exotic options. Practitioners favor FDM for calculating the Greeks of ELNs, which are essential for risk management and hedging. However, FDM's accuracy depends on grid size and spacing, and it often requires grid adjustments to manage continuous barriers, especially in multi-dimensional applications. As grid adjustments increase, computational costs also rise, making FDM less practical for complex derivatives with high-dimensional structures. Meanwhile, MCS offers flexibility in modeling complex

payoff structures, such as those with multiple paths and varied outcomes, making it suitable for ELN pricing. However, MCS suffers from high variance in its results, which increases as the number of simulated paths rises. MCS is inefficient for derivatives with early exercise features, such as American and Bermudan options, as it assumes a continuous time horizon, requiring additional computations to determine the optimal exercise point, which slows convergence.

To address the limitations of these traditional methods, we introduce the FIM as an efficient alternative for ELN valuation. FIM offers distinct advantages over FDM and MCS, particularly in handling the unique features inherent in ELNs. Unlike FDM, which relies on meticulous grid adjustments to accurately handle continuous barriers, FIM simplifies this process, eliminating the need for complex grid configurations. This efficiency significantly reduces computational costs and enhances stability across various boundary conditions, particularly in multi-dimensional applications. FIM's integration-based framework is highly effective for capturing the intricate payoff structures of ELNs, including step-down strike rates, knock-in barriers, and binary features that determine returns based on threshold conditions. FIM's inherent flexibility enables it to manage these conditions accurately, where FDM or MCS might face convergence or stability challenges. Unlike MCS, which are prone to high variance due to path dependencies, FIM provides deterministic outcomes, offering consistent results across calculations. This consistency is especially beneficial for ELNs with early redemption features, avoiding extensive variance reduction techniques typically required in MCS. Additionally, FIM excels in calculating Greeks with high precision, supporting robust risk management and hedging strategies by accurately capturing sensitivity to market conditions.

In summary, FIM addresses the primary limitations of FDM and MCS, offering an accurate and stable approach for valuing ELNs with complex structures. In the following sections, we describe the FIM methodology in detail and provide numerical results to validate its effectiveness as a practical and accurate approach for ELN valuation.

2.2. Finite integration method

In previous works [36, 37], we presented the FIM and applied it to evaluate and hedge standard financial products. Our investigation demonstrated that FIM outperforms the Crank-Nicolson scheme-based FDM in accurately pricing European and American options with one underlying asset. Moreover, in a subsequent inquiry, we compared FIM with the implicit scheme-based operator splitting method(OSM) in pricing binary and European options with two underlying assets. The results suggested that FIM provides precise and stable financial instrument valuations and is adaptable to assess multi-dimensional derivatives. Consequently, FIM confers various benefits for financial instrument valuation over other alternative methods.

When feasible, the FIM aims to minimize the reliance on numerical routines by conducting analytic computations. Assuming that the stock price $S(t)$ follows a geometric Brownian motion, the security value $V(t, S(t))$ satisfies the Black-Scholes PDE. The solution of this PDE entails a discounted integration of the future security values multiplied by the transitional probability density functions. There are several ways of computing this integral, including numerical evaluation or approximation of the integrand for analytical integration. Although both approaches are reasonable and functional, a superior alternative exists for situations where the transitional probability density functions exhibit log-normal distribution patterns, namely, the FIM. Unlike full integrand approximation, FIM applies quadratic piecewise approximations only to future security values. The requisite computation involves

the integration of the exponential term multiplied by the at-most quadratic polynomial, which is then analytically integrated by FIM, as opposed to numerical methods. In the first paper's appendix [36], we have summarized the formulas utilized in the FIM approach.

Figure 2 illustrates a single backward step of the FIM. The state space is partitioned into intervals $I_j = [s_j, s_{j+1}]$, and at time $t + \Delta t$ the future value $V(t + \Delta t, \cdot)$ is approximated on each I_j by a quadratic polynomial. For a current state s at time t, FIM computes the discounted conditional expectation by integrating this polynomial surrogate against the one-step lognormal transition density $p(s' \mid s; \Delta t)$ over each I_j and summing the contributions across j, which yields $V(t, s)$. Equivalently, the per-interval update reduces to a closed-form linear combination of three truncated lognormal moments (corresponding to 1, s', and s'^2), so the convection-diffusion operator is advanced without time-discretization error and with high spatial accuracy. In higher dimensions, the same one-step construction is applied axis by axis with the remaining coordinates held fixed (operator splitting), and the correlation contribution is then incorporated by the time-shifted cross (heat-source) update specified in Algorithm 1.

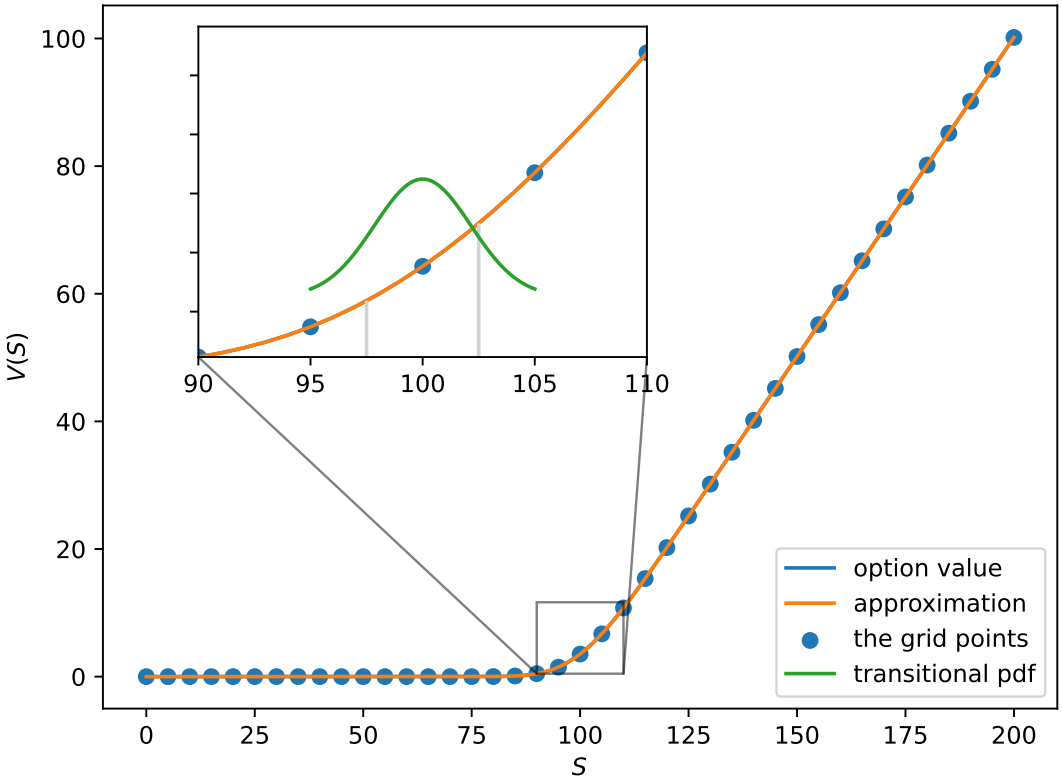

Figure 2. This figure illustrates the evaluation process of a European option using FIM. The feasible range of stock prices is divided into intervals, and the blue curve represents the option price at time $t + \Delta t$. The orange curve approximates the option price values using piecewise quadratic functions. The green curve shows the transition probability density function. FIM calculates the integration of the orange approximate option price multiplied by the transition probability density function over specific subintervals. The European option price, $V(t, s)$, is obtained by summing the integral values for all subintervals.

Algorithm 1 FIM-2D: Operator splitting with heat-source correction

Given r (risk-free rate), σ_x, σ_y (volatilities), ρ (correlation); spatial grids $\{x_i\}_{i=0}^{N_x}$, $\{y_j\}_{j=0}^{N_y}$ with spacings $\Delta x, \Delta y$; time grid $\{t_k\}_{k=0}^{n_t}$ with step Δt; terminal payoff $\Phi(x, y)$.

Set $\gamma \leftarrow r/2, \quad \eta \leftarrow \dfrac{e^{\gamma \Delta t} - 1}{\gamma}, \quad V_{i,j}^{n_t} \leftarrow \Phi(x_i, y_j)$

Notation. $V_{i,j}^k := V(t_k, x_i, y_j)$; we use intermediate arrays F_1^k, F_2^k at time t_k.

Mixed difference. For any grid function F, define the centered mixed difference at t_{k+1} by

$$\left(D_{xy}F\right)_{i,j}^{k+1} = \frac{F_{i+1,j+1}^{k+1} - F_{i+1,j-1}^{k+1} - F_{i-1,j+1}^{k+1} + F_{i-1,j-1}^{k+1}}{4\,\Delta x\,\Delta y},$$

using one-sided variants on boundaries.

for $k = n_t - 1, \ldots, 0$ **do**

Problem 1 (x–update). Let $F_1^{k+1} \leftarrow V^{k+1}$.

Heat source (from the cross term $\rho\,\sigma_x\sigma_y\,xy\,\partial^2/(\partial x\,\partial y)$):

$$h_1^{k+1}(x_i, y_j) = \tfrac{1}{2}\,\rho\,\sigma_x\sigma_y\,x_i y_j\,\left(D_{xy}F_1\right)_{i,j}^{k+1}.$$

FIM-1D along x with discount γ:

$$F_1^k \;\leftarrow\; \mathrm{FIM1D}_x\Big(F_1^{k+1} + \eta\,h_1^{k+1};\ \gamma, \Delta t, \Delta x\Big).$$

Problem 2 (y-update). Set $F_2^{k+1} \leftarrow F_1^k$.

Heat source (recomputed at t_{k+1}):

$$h_2^{k+1}(x_i, y_j) = \tfrac{1}{2}\,\rho\,\sigma_x\sigma_y\,x_i y_j\,\left(D_{xy}F_2\right)_{i,j}^{k+1}.$$

FIM-1D along y with discount γ:

$$V^k \;\leftarrow\; \mathrm{FIM1D}_y\Big(F_2^{k+1} + \eta\,h_2^{k+1};\ \gamma, \Delta t, \Delta y\Big).$$

(Product events) If t_k is an observation date, apply barrier checks / coupons / early redemption to V^k.

Return V^0.

In dimensions $k > 1$, we compute the conditional expectation by repeating the one-dimensional FIM integration along each asset axis while keeping the remaining coordinates fixed; that is, on every axis we fit the quadratic surrogate of $V(t + \Delta t, \cdot)$ on each interval and integrate it analytically against the one-step lognormal density. Correlation is incorporated afterward through the cross (heat-source) term described in Algorithm 1, where the mixed derivatives are evaluated by centered differences at the level $t + \Delta t$ and the update is added once per step with discounting. This procedure evaluates the multi-asset expectation with correlated assets without forming a full k-dimensional quadrature.

We advance one time slab $[t_k, t_{k+1}]$ with operator splitting and a time-shifted heat source. Set $\gamma = r/2$ and $\eta = (e^{\gamma \Delta t} - 1)/\gamma$, and perform two one-dimensional FIM sweeps.

(i) x-update: initialize $F_1^{k+1} \leftarrow V^{k+1}$. On the grid at t_{k+1} compute the centered mixed difference $(D_{xy}F_1)_{i,j}^{k+1}$ (as defined in Algorithm 1), and set $h_1^{k+1}(x_i, y_j) = \frac{1}{2}\,\rho\,\sigma_x\sigma_y\,x_i y_j\,(D_{xy}F_1)_{i,j}^{k+1}$. Apply 1D FIM in x with discount γ to $F_1^{k+1} + \eta\,h_1^{k+1}$ (piecewise quadratics in x, closed-form integration against

the one-step lognormal transition, then multiply by $e^{-\gamma\Delta t}$) to obtain F_1^k.

(ii) y-update: set $F_2^{k+1} \leftarrow F_1^k$, recompute the centered mixed difference $(D_{xy}F_2)_{i,j}^{k+1}$ (as defined in Algorithm 1) and $h_2^{k+1}(x_i, y_j) = \frac{1}{2}\,\rho\,\sigma_x\sigma_y\,x_i y_j\,(D_{xy}F_2)_{i,j}^{k+1}$ at t_{k+1}, and apply 1D FIM in y with discount γ to $F_2^{k+1} + \eta\,h_2^{k+1}$ to get V^k. If t_k is an observation date, product events are applied to V^k.

With this construction, the convection-diffusion and discount parts are handled analytically along each axis, and the correlation ρ is incorporated at each step via the explicit heat-source evaluated at the shifted level t_{k+1} (through the centered mixed difference D_{xy}). Theoretical guarantees from [36, 37] apply: In the multi-asset Black–Scholes setting under operator splitting the scheme is unconditionally stable; the convection-diffusion component retains third-order spatial accuracy $O(\Delta S^3)$, while the cross (heat-source) update contributes an additional term of order $\rho\,[O(\Delta t^2) + O(\Delta t\,\Delta S^2)]$. Moreover, for the convection-diffusion part the time-discretization error is zero because the conditional expectation over one step is evaluated analytically. These orders are summarized in the analysis and tables of [37].

3. Results

Section 2.1 comprehensively describes the ELNs and their connections to binary and barrier options. Section 2.2 introduces the fundamental concept of FIM. This section evaluates the accuracy of FIM compared to the implicit FDM for three specific financial instruments: A one-dimensional down-and-out put option, a two-dimensional binary call option, and the ELNs, which are the primary focus of interest. Previous research has established FIM's theoretical and empirical stability and accuracy regarding standard financial products involving one and two underlying assets. In this section, we present the effectiveness of FIM in handling more exotic financial derivatives that encompass digital payoffs and barriers. Furthermore, we extend our previous investigations to incorporate the ELNs, widely popular financial products in the current marketplace.

3.1. Barrier and binary option experiments

This study's central focus revolves around assessing the ELNs that involve two underlying assets. However, our analysis begins by examining barrier options with a single asset and binary options with two assets. To this end, we utilize the formulas outlined in the book authored by Haug [40] for standard barrier options featuring one underlying asset and binary options with two underlying assets. Note that barrier options with multiple underlying assets lack closed-form solutions. Consequently, we conduct an error analysis of a down-and-out put option with only a single underlying asset, not two.

We assess the effectiveness of the FDM and the FIM in analyzing financial derivatives. We evaluate a barrier option with a single underlying asset using the implicit FDM and the FIM 1D. Furthermore, we conduct a comparative investigation of the outcomes generated by the FIM 2D and the implicit OSM to analyze a binary option with two underlying assets. Moving forward, we will use the acronym FIM to refer to FIM 1D and FIM 2D, while the abbreviation FDM will encompass both the implicit FDM and the implicit OSM.

Table 2 presents a comprehensive overview of the maximum errors encountered when employing FDM and FIM in valuing a barrier option with a single underlying asset and a binary option with two underlying assets under standard conditions, where the strike price is 100, the time to maturity is one month, the risk-free interest rate is 2%, and the volatility is 30%. For the binary option involving two assets, a correlation coefficient of 0.3 is assumed, while for the barrier option, the barrier is 60.

Additionally, we set the maximum underlying asset price to be 300, with 30 time grid intervals and 300 price grid intervals utilized.

Table 2. This table reports the maximum errors encountered when utilizing FDM and FIM to value a barrier option with a single underlying asset and a binary option with two underlying assets. We evaluate these options assuming a strike price of 100, a one-month time to maturity, a risk-free interest rate of 2%, and volatility of 30%. We consider a correlation coefficient of 0.3 for the binary option, while the barrier option had a barrier level of 60. We set the maximum underlying asset price to 300 and employ 30 time grid intervals and 300 price grid intervals.
Note: Table 2 reports the maximum pricing error over the asset grid $S \in [0, 300]$, hence it does not depend on the current spot S_0. For reproducibility in Figure 3, we use $S_0 = 65$.

	barrier option		binary option	
	FDM	FIM	FDM	FIM
price	1.714×10^{0}	$\mathbf{7.368 \times 10^{-1}}$	4.127×10^{-1}	$\mathbf{4.831 \times 10^{-2}}$
delta	8.568×10^{-1}	$\mathbf{3.684 \times 10^{-1}}$	6.554×10^{-2}	$\mathbf{7.278 \times 10^{-3}}$
gamma	1.744×10^{0}	$\mathbf{8.879 \times 10^{-1}}$	6.875×10^{-3}	$\mathbf{8.945 \times 10^{-4}}$
vega	6.843×10^{0}	$\mathbf{6.428 \times 10^{0}}$	1.774×10^{0}	$\mathbf{4.590 \times 10^{-1}}$

The accuracy assessment involves computing the price error, which reflects the discrepancy between the option's price obtained from each method and its corresponding closed-form solution. Furthermore, we evaluate the delta, gamma, and vega sensitivity errors to gauge inconsistencies relative to the Greeks derived from the closed-form solution. Results demonstrate that FIM achieves notably higher precision in the pricing of binary options than FDM, as evidenced by an approximate ten-fold reduction in price and sensitivity errors. However, when analyzing barrier options, FIM's superiority over FDM is marginally enhanced, with only slight improvements in error rates. This phenomenon is due to the barrier discontinuity, which imparts a less smooth solution and reduces FIM's convergence rate. While FIM offers greater accuracy than FDM, its advantage in pricing barrier options with continuous barriers remains relatively modest and presents challenges.

Pricing barrier options numerically presents a challenging task, and errors that arise from the discretization of the time axis are particularly significant when pricing options with a continuous barrier. In order to assess the accuracy of FIM for pricing such options on a discretized grid, we compare its convergence rates against those of FDM. We run the experiments under the same conditions of Table 2 except for several different time grid intervals used to observe how fast time discretization error diminishes. We discretize the time axis using a varying number of time intervals, ranging from 2 to 60, leading to time interval lengths of 15, 6, 3, 2, 1, and 0.5 days, respectively, according to the 30/360-day counting convention.

Figure 3 visualizes the errors observed when the underlying asset's current price is 65, very close to the barrier of 60, thereby facilitating a more detailed analysis of the variations in error when the current price is close to the barrier. The results unequivocally show that reducing the time step size reduces the errors associated with the price, delta, and gamma values of both FDM and FIM. The square-marked curves of FIM plotted in Figure 3 converge to the benchmark horizontal lines at 20.3442, 2.7069, and −0.6393, respectively, faster than the triangle-marked curves of FDM, revealing

the superior convergence rate of FIM over FDM to the benchmark. Notably, the square-marked curves of FIM exhibit a higher error reduction rate than FDM. Specifically, to achieve an error level of 10^{-2} when determining the price and sensitivities of a barrier option with a one-month expiration, FIM requires only a total of 60 time steps, whereas FDM requires more. This FIM's superior convergence over FDM aligns with the findings in [36].

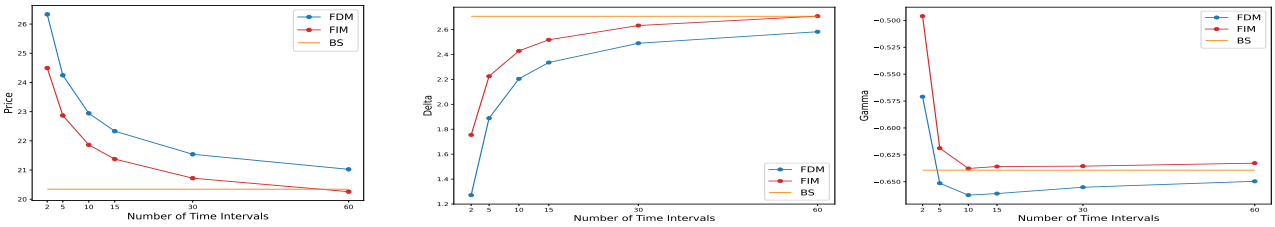

(a) Price **(b)** Delta **(c)** Gamma

Figure 3. Error analysis for barrier option pricing. This figure presents an analysis of errors observed when the underlying asset's current price is 65, close to the barrier level of 60. The strike price is 100, the barrier is 60, and the time to maturity is 0.5. We assume that the underlying stock price is 65, the stock volatility is 30%, and the risk-free interest rate is 2%. The square-marked curves representing FIM converge faster to the benchmark horizontal lines at 20.3442, 2.7069, and −0.6393 compared to the triangle-marked curves of FDM. We fix the number of asset intervals to 150, and the maximum asset grid value is 150.

Figure 4 compares price, delta, and gamma error surfaces obtained using FDM and FIM. The analysis focuses on the evolution of errors as the algorithms iteratively calculate values from maturity to the current time. The asset step size is set to one, while the time step size corresponds to one day. To see the error propagation closely, we restrict the asset axis from 50 to 80, encompassing a barrier level of 60 where a substantial price change occurs. The primary focus of our investigation lies in the temporal grid points preceding maturity, as the values at maturity are initially assigned based on the predetermined payoff. Since there is no price uncertainty at maturity, we restrict the time axis by excluding the final time step associated with the expiration. To facilitate a meaningful comparison, we overlay the error surfaces generated by the FDM in blue with those produced by the FIM in red. The error surfaces depicted in Figure 4 demonstrate that significant errors occur near the barrier. FIM initially exhibits fewer minor errors than FDM. As the iterations progress, these errors gradually diminish from maturity to the present moment. Notably, the current price, delta, and gamma values obtained from FIM exhibit errors that are at most half the magnitude of those generated by FDM, as displayed in Figure 5, where we present the current price and Greek values for both FDM and FIM.

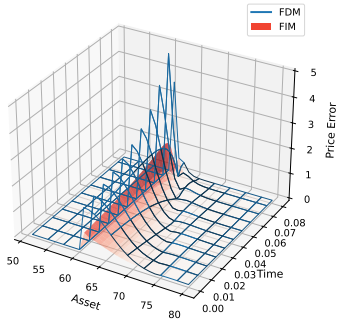

(a) Price

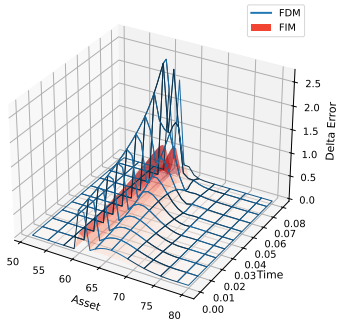

(b) Delta

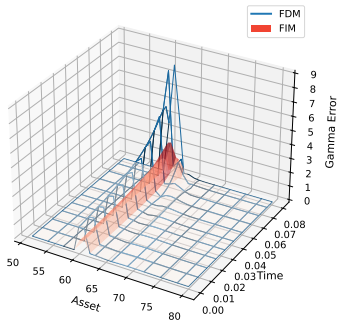

(c) Gamma

Figure 4. Comparative analysis of absolute error surfaces for the barrier option. This figure compares price, delta, and gamma error surfaces obtained using FDM and FIM. The analysis focuses on the evolution of errors as the algorithms iteratively calculate values from maturity to the current time. The asset step size is one, and the time step size corresponds to one day. The asset axis is restricted from 50 to 80, including the barrier level of 60, to observe significant price changes. We present the error surfaces obtained from FDM in blue and FIM in red. Initially, FIM exhibits smaller errors compared to FDM. As iterations progress, these errors gradually decrease from maturity to the present.

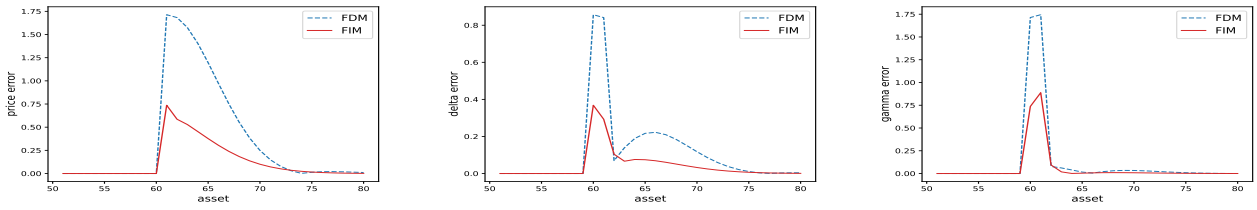

(a) Price **(b)** Delta **(c)** Gamma

Figure 5. FDM and FIM absolute error comparison at present. This figure compares the absolute errors of the current price, delta, and gamma values obtained from FDM (solid lines) and FIM (dotted lines). The errors of FIM are consistently smaller, with at most half the magnitude of those generated by FDM.

We clarify why FIM behaves favorably in the vicinity of the knock-in barrier. In our implementation, the one-step risk-neutral expectation is evaluated in closed form, and barrier/early-redemption events are applied only at observation dates after this update. Because the integral operator advances the convection-diffusion part analytically, the value surface does not require the barrier to align with grid nodes and is less prone to numerical diffusion around the activation threshold. Consistent with this mechanism, our barrier-option experiment shows that—as the time and asset grids are refined—FIM converges reliably to the analytical reference and attains smaller errors near the barrier than the finite-difference scheme. In particular, the integral-based update delivers stable prices and Greeks for discontinuous payoff structures without resorting to barrier-aligned meshes.

Although the inherent discontinuous boundary conditions of barrier options can make results less smooth and somewhat limit the performance improvement of FIM, the method still showcases its ability to outperform FDM in both convergence speed and error reduction. This observation highlights challenges in addressing discontinuities but also reinforces FIM's computational strengths and potential for further enhancement.

3.2. Equity-linked note experiments

This subsection prices a k-dimensional step-down ELN with a knock-in barrier by applying the FIM-based backward recursion in Algorithm 2. At each time node, the FIM produces the full value surface on the state grid; from this surface, we extract prices and the main sensitivities (delta and the diagonal gamma), and we validate them against MCS results under identical model parameters. The mixed second derivative with respect to the two underlyings can be obtained on the same FIM surface using the same finite-difference machinery as for the diagonal gamma (centered differences with the same step size, with standard one-sided variants near boundaries). As the number of MCS samples increases, the discrepancies between FIM and MCS shrink, which is consistent with the convergence properties of our scheme; accordingly, the figures focus on price, delta, and the diagonal gamma.

We benchmark the FIM results against a MCS engine under the same risk-neutral geometric brownian motion model. Correlated shocks are generated by a Cholesky factor of the target correlation matrix. The time grid explicitly includes all observation dates; product events are applied only at those dates and in the following order: (i) early redemption check and immediate termination if triggered, with discounting on the event date; (ii) otherwise, we track the running minimum to determine knock-in at

maturity. Greeks (delta, gamma) are estimated by central differences with symmetric spot bumps while reusing the same random numbers across base/up/down runs (common random numbers).

We discretize time as $0 = t_0 < t_1 < \cdots < t_m = T_n$ and include all observation (early-redemption and barrier-monitoring) dates $\mathcal{T}_{\text{obs}} = \{T_1, \ldots, T_n\} \subset \{t_j\}$ on the time grid. For each asset $i = 1, \ldots, k$, the state axis is partitioned as $0 = x_{i,0} < x_{i,1} < \cdots < x_{i,\ell_i} = x_{i,\max}$. We work with normalized returns $\mathbf{x} = (x_1, \ldots, x_k)$ (e.g., $x_i = S_i/S_i(0)$), so that early-redemption thresholds $\{K_j\}$ and the knock-in barrier B are evaluated on $\min(\mathbf{x})$ at the observation dates.

At each time grid point t_j, the FIM algorithm keeps tracking two price vectors $U(\mathbf{x})$ and $V(\mathbf{x})$ when $\mathbf{x} = (x_1, x_2, \ldots, x_k)$ represents the k number of underlying asset prices at t_j. The first price vector $U(\mathbf{x})$ records the ELN valuation when none of the underlying asset prices has touched the knock-in barrier up to the current evaluation time t_j, whereas the second $V(\mathbf{x})$ traces the ELN price of the other barrier-hitting case.

Algorithm 2 FIM Algorithm for Pricing an n-Dimensional Step-Down ELN with a Knock-in Barrier

State arrays: U (no knock-in), V (knock-in) on the d-asset grid

Assume: observation dates $\mathcal{T}_{\text{obs}} \subset (0, T_n)$, and $B < K_j$ (events are disjoint)

function FIM(X)

Operator-split FIM-2D/ND: axis-wise analytic expectation with discounting, then time-shifted heat-source (cross) update at t'. One-sided stencils at boundaries.

return updated X

Initialization at T_n: $U \leftarrow \Phi_U$, $V \leftarrow \Phi_V$

for $t = t_{m-1}, t_{m-2}, \ldots, t_0$ **do** ▷ backward in time

$U \leftarrow \text{FIM}(U), \quad V \leftarrow \text{FIM}(V)$ ▷ propagate one step

if $t \in \mathcal{T}_{\text{obs}}$ **then**

for each grid node **x do**

if $\min(\mathbf{x}) \le B$ **then** ▷ knock-in barrier (discrete monitoring)

$U(\mathbf{x}) \leftarrow V(\mathbf{x})$

if $\min(\mathbf{x}) \ge K(t)$ **then** ▷ early redemption at t

$U(\mathbf{x}) \leftarrow (1 + r(t))N, \quad V(\mathbf{x}) \leftarrow (1 + r(t))N$

Output: $U(t_0, \cdot)$ as the present value; Greeks by centered differences on $U(t_0, \cdot)$

(i) **States.** U is the no-knock-in state and V the knock-in state, both defined on the same d-asset Cartesian grid. At maturity T_n, the two states are fully specified by Φ_U, Φ_V; hence, no copy step is needed at T_n.

(ii) **Propagation (FIM).** FIM$(\cdot)$ applies the finite-integration update over one time step: an axis-wise analytic expectation under the one-step lognormal transition with discounting, followed by a time-shifted cross (heat-source) correction for correlation using a centered stencil (one-sided at boundaries). This is the same operator-splitting design used in our 2D FIM reference.

(iii) **Event timing.** Product events are processed only on observation dates after the propagation at t_j: first the discrete barrier (knock-in) check, then early redemption. We assume $B < K_j$ for all j, so the two events are disjoint and cannot trigger simultaneously.

(iv) **Early redemption payoff.** When $\min(\mathbf{x}) \ge K_j$ at an observation date t_j, both U and V are set to the coupon payoff $(1 + r_j)N$ at t_j (no additional discount is applied after assignment).

(v) **Price and Greeks.** The ELN price is $U(t_0, \cdot)$ at the present time t_0. Greeks are evaluated by centered differences on $U(t_0, \cdot)$ with one-sided stencils at the boundaries.

After applying the barrier/early-redemption events at $t_j \in \mathcal{T}_{\text{obs}}$, the next-step piecewise quadratic surrogates used by FIM are re-fitted on the updated grid values. This ensures that the update $U(\mathbf{x}) \leftarrow V(\mathbf{x})$ and coupon assignments are consistently coupled with the FIM's piecewise quadratic integration in the subsequent step.

At maturity T_n, the terminal payoffs are fully specified on the returns grid by Φ_U and Φ_V in Eqs (3.1)–(3.2). In particular, when $\min(\mathbf{x}) \geq K_n$ both states pay the last redemption $(1 + r_n)N$; when $\min(\mathbf{x}) > B$ but $< K_n$, the no-knock-in state follows the dummy payoff $(1 + d)N$ while the knock-in state follows $N \cdot \min(\mathbf{x})$; otherwise both states follow $N \cdot \min(\mathbf{x})$. No copy step is needed because both U and V are defined on the entire grid at T_n.

$$\Phi_U(\mathbf{x}) := \begin{cases} (1 + r_n)N & \text{if } \min(\mathbf{x}) \geq K_n \\ (1 + d)N & \text{if } \min(\mathbf{x}) > B \\ \min(\mathbf{x}) & \text{otherwise} \end{cases} \tag{3.1}$$

$$\Phi_V(\mathbf{x}) := \begin{cases} (1 + r_n)N & \text{if } \min(\mathbf{x}) \geq K_n \\ \min(\mathbf{x}) & \text{otherwise} \end{cases}. \tag{3.2}$$

For each step $t_{j+1} \to t_j$, we first propagate U and V by Algorithm 1 (axis-wise analytic expectation with discounting followed by the time-shifted cross update). If $t_j \in \mathcal{T}_{\text{obs}}$, we then apply the product events on the grid: (i) knock-in—set $U(\mathbf{x}) \leftarrow V(\mathbf{x})$ whenever $\min(\mathbf{x}) \leq B$; (ii) early redemption—set $U(\mathbf{x}) = V(\mathbf{x}) = (1 + r_j)N$ whenever $\min(\mathbf{x}) \geq K_j$. The piecewise-quadratic surrogates used by FIM in the next step are refitted on these updated grid values.

The ELN pricer, therefore, consists of four stages: Initialization at maturity, FIM backward propagation, barrier validation, and early-redemption assignment—applied in this fixed order at the observation dates. Other ELN variants (e.g., step-up, lizard) are handled by the same numerical core with only the event logic modified at the observation dates.

To facilitate visualization, we now examine the algorithm's application in a 2-dimensional asset space. Following the prescribed steps outlined in the FIM algorithm of pricing a step-down ELN with a knock-in barrier, the FIM algorithm generates a comprehensive current price surface denoted as $U(\mathbf{x})$, encompassing all the domain points within the asset space. In order to provide a visual representation, we construct the current price surface in Figure 6 for an ELN with a maturity of three years, as shown in Figure 1, where the notional value N is 100. The relevant parameters include a risk-free interest rate of 2%, a volatility of 30%, and a correlation coefficient of 0.3. We choose the time step size as one day, the asset step size as 1, and the maximum asset price as 300. Notably, the price of 89.0577 at the current initial spots, represented by $\mathbf{x} = (100, 100)$, is indicated with a star symbol to highlight its significance.

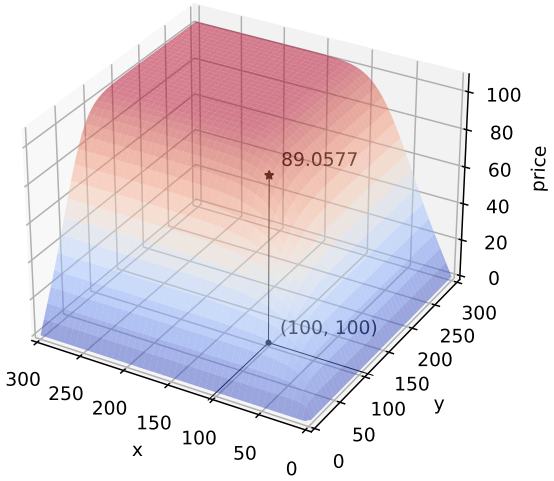

Figure 6. Current price surface of a step-down ELN with a knock-in barrier. This figure presents the current price surface, denoted as $U(x, y)$, generated by the FIM algorithm for a step-down ELN with a maturity of three years. The notional value is 100, and the relevant parameters include a risk-free interest rate of 2%, a volatility of 30%, and a correlation coefficient of 0.3. The time step size is set as one day, the asset step size is 1, and the maximum asset price is 300. The price of 89.0577 at the initial spot $(x, y) = (100, 100)$ is marked with a star symbol to emphasize its significance. Here, x and y denote the current prices of the first and second underlying assets, respectively.

Given the absence of a closed-form solution to ascertain the price and sensitivity of an ELN, we have chosen to employ MCS as a benchmark against the FIM. MCS is widely adopted in practical financial applications owing to its adaptability and efficacy in handling complex financial instruments. We employ first-order and second-order central difference approximations with a step size of $ds = 1$ to compute the numerical delta and gamma. The sensitivity analysis exhibits symmetry in our experimental configuration, where the underlying assets have equivalent volatilities. So, we evaluate sensitivity along the x-axis only at the coordinate point $(x, y) = (100, 100)$.

Since there is no closed-form for ELN prices and Greeks, we use MCS as a benchmark. The MCS uses exact one-step sampling for the geometric brownian motion on the same time grid as FIM and applies events only at the observation dates (early redemption first, then knock-in tracking to maturity). Discounting is done on the event date. We report the number of paths, the time step, the count, and the random seeds used in each experiment. Greeks are computed by central differences with symmetric spot bumps, and we reuse the same random numbers across base/up/down runs to reduce variance. These settings make the MCS-FIM comparison reproducible and aligned with the product logic.

The findings are depicted through box plots, as illustrated in Figure 7. To visualize the sampling dispersion of the MCS prices and sensitivities, we perform one hundred independent replications for each fixed sample size 10^4, 5×10^4, and 10^5. The box plots summarize the interquartile range (Q1–Q3) and the median across replications. FIM's price, delta, and gamma values are always within the Q1–Q3 band, supporting the accuracy of the FIM algorithm. The MCS medians differ from the FIM values because of sampling variability, but for the cases considered, they are very close. Moreover, the Q1–Q3

band narrows as the number of samples increases; even then, the FIM values remain inside the Q1–Q3 band and stay very close to the MCS medians, providing strong evidence for the reliability of FIM in pricing and computing hedging parameters.

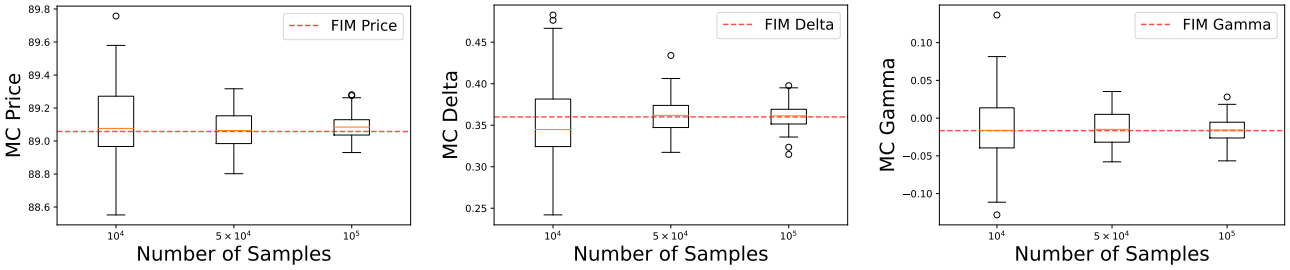

(a) Price **(b)** Delta **(c)** Gamma

Figure 7. This figure presents box plots that depict the findings of the comparison between FIM and MCS conducted for pricing and computing hedging parameters of a step-down ELN. One hundred simulations are performed with different random seeds, using fixed sample sizes of 10^4, 5×10^4, and 10^5. The FIM algorithm consistently yields price, delta, and gamma values within the Q_1–Q_3 confidence intervals.

The previous experiment involved a daily MCS and FIM's one-day time step size. While the MCS does not restrict possible stock prices, the FIM's asset step size is determined to 1. To compare the results of the two methods under similar conditions of the underlying asset price distribution, we analyze the convergence of FIM's price and sensitivities by varying the number of asset steps. Table 3 summarizes the findings of this experiment; the FIM computes prices and sensitivities of the ELN using different numbers of asset grid points while the number of time grid points remains at 1080. FIM's prices and sensitivities remain stable while the number of asset steps changes, suggesting that asset step size of 1 is a sound choice for the FIM computation.

Table 3. Convergence analysis of FIM with varying the number of asset grid points. This table provides the results of a convergence analysis conducted on FIM's price and sensitivities, considering different numbers of asset grid points while maintaining the number of time grid points constantly at 1080. The findings demonstrate that FIM's prices and sensitivities exhibit stability and consistency across different numbers of asset steps.

Grid points		Price	Delta	Gamma
time	asset			
1080	300	89.0577	0.3600	−0.0166
1080	600	89.0667	0.3599	−0.0166
1080	900	89.0705	0.3598	−0.0166
1080	1200	89.0721	0.3598	−0.0166

Figure 8 reports single-threaded runtimes under identical settings. In panel 8(a), FIM increases roughly linearly with the number of time steps n_t, remaining in a seconds-to-tens-of-seconds range over our sweep, while MCS grows more steeply with n_t. In panel 8(b), FIM rises predictably with the spatial grid size n_s, whereas MCS shows little dependence on n_s. Each marker denotes the median across at

least three independent runs. For a like-for-like accuracy comparison with FDM, see the Pareto-frontier results below.

Figure 9(a)–(c) plot per-method Pareto frontiers, retaining only non-dominated pairs (error, runtime). In Barrier1D, relative to the closed-form reference, FIM attains very tight tolerances within seconds, whereas OSM reaches millisecond-level runtimes at moderate error levels. In Binary2D and Euro2D, where the fronts overlap in error, OSM is faster at matched accuracy, while FIM extends the frontier toward tighter tolerances when run on finer settings. These results complement the ELN scaling by indicating when each method is preferable: FIM for tight accuracy targets and path-dependent cases; OSM for minimal latency at moderate accuracy.

Setup note. All experiments are run on the same workstation (macOS 15.6.1, ARM64, 8 logical CPUs). We use a single CPU core for all timings and report the median over at least three independent runs.

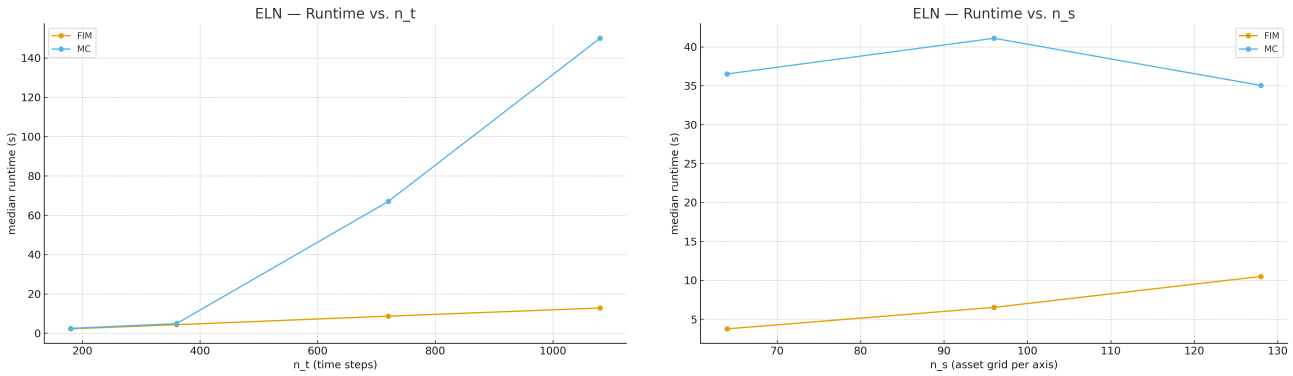

(a) ELN — Runtime vs. n_t

(b) ELN — Runtime vs. n_s

Figure 8. ELN runtime scaling (single core). Runtimes are measured on the same machine using one CPU core. Each marker shows the median wall-clock time over at least three independent runs. Panel (a) varies the number of time steps n_t; panel (b) varies the asset-grid size n_s. Briefly, FIM grows roughly linearly with n_t, while MCS increases more steeply; with n_s, FIM increases predictably and MCS is largely insensitive. The plot shows scaling in the number of time steps for a fixed 2-asset grid; the overall runtime also increases with the grid size/dimension. The total runtime scales as $O(n_t\, n_{\text{tot}})$, where $n_{\text{tot}} = \prod_{i=1}^{k} n_{s,i}$ is the total number of spatial grid nodes.

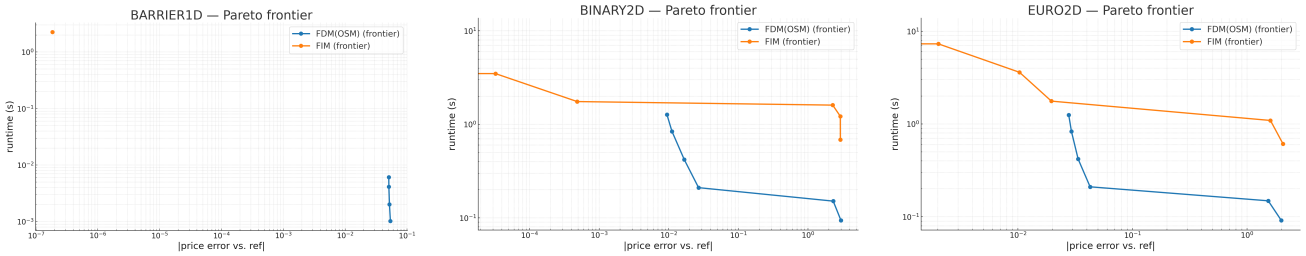

(a) Barrier1D — Pareto frontier **(b)** Binary2D — Pareto frontier **(c)** Euro2D — Pareto frontier

Figure 9. Runtime–accuracy Pareto frontiers(both axes logarithmic). A Pareto frontier keeps, for each method, only those points for which no other tested configuration is both faster and more accurate; it shows the best runtime we observed at each error level. Errors use $|V - V_{\text{ref}}|$, where V_{ref} is the reference price: the analytical Black–Scholes value for Barrier1D, and the finest-grid price from our sweep for Binary2D/Euro2D. All runs use one CPU core; each marker is the median over at least three repetitions. Briefly, Barrier1D shows separate accuracy bands across methods; in Binary2D/Euro2D, frontiers overlap in error and expose the time-accuracy trade-offs.

4. Conclusions

In this study, we introduced the FIM as an efficient and accurate numerical framework for pricing and hedging ELNs. ELNs are structured products characterized by complex payoff mechanisms, including barrier and binary features, which make their valuation particularly challenging. Our numerical experiments demonstrated that FIM consistently outperforms the FDM in terms of pricing accuracy and convergence speed, especially for barrier options with a single underlying asset and binary calls with two underlying assets. As the number of time grid points increases, FIM exhibits superior convergence toward the benchmark closed-form solutions.

Moreover, we observed that the prices and Greeks computed using FIM align closely with those obtained from MCS, further validating the reliability and robustness of the FIM approach for ELN valuation and risk analysis. The proposed algorithm for step-down ELNs is sufficiently flexible to accommodate a variety of payoff structures, making it applicable to a broad class of structured financial products.

Overall, our findings establish the FIM as a practical, efficient alternative to conventional numerical schemes for pricing both vanilla and exotic derivatives, including binary options, barrier options, and ELNs. Moreover, due to its semi-discrete formulation, the FIM is naturally extendable to models with non-constant coefficients, such as those incorporating stochastic or local volatility (e.g., Heston or stochastic alpha beta rho model (SABR)), without requiring structural modifications to the algorithm. Future research could explore the extension of the FIM framework to a broader class of structured products, including step-up, step-down, and lizard ELNs, as well as other exotic options such as Asian options and path-dependent derivatives. These directions underscore the potential of FIM to further advance numerical techniques in structured finance.

Author contributions

Yejin Kim: Conceptualization, methodology, software, validation, formal analysis, data curation, investigation, visualization, writing – original draft; Wooyeol Jeong: Methodology, validation, formal analysis, investigation, visualization, writing – original draft, writing – review and editing; Sungchul Lee: Supervision, writing – review and editing. All authors have read and approved the final version of the manuscript for publication.

Use of Generative-AI tools declaration

The authors declare they have not used Artificial Intelligence (AI) tools in the creation of this article.

Acknowledgments

This work was supported by the National Research Foundation of Korea (NRF) grant funded by the Korea government (Grant No. RS-2024-00456958).

Conflict of interest

The authors declare that they have no conflicts of interest in this paper.

References

1. F. Black, M. Scholes, The pricing of options and corporate liabilities, *J. Polit. Econ.*, **81** (1973), 637–654. https://doi.org/10.1086/260062
2. R. C. Merton, Theory of rational option pricing, *Bell J. Econ. Manag. Sci.*, **4** (1973), 141–183. https://doi.org/10.1098/rspb.1973.0010
3. J. C. Cox, S. A. Ross, M. Rubinstein, Option pricing: A simplified approach, *J. Financ. Econ.*, **7** (1979), 229–263. https://doi.org/10.1016/0304-405X(79)90015-1
4. F. Soleymani, B. N. Saray, Pricing the financial Heston–Hull–White model with arbitrary correlation factors via an adaptive FDM, *Comput. Math. Appl.*, **77** (2019), 1107–1123. https://doi.org/10.1016/j.camwa.2018.10.047
5. M. L. Mao, W. S. Wang, T. H. Tian, L. H. Wang, Adaptive option pricing based on a posteriori error estimates for fully discrete finite difference methods, *J. Comput. Appl. Math.*, **460** (2025). https://doi.org/10.1016/j.cam.2024.116407
6. J. Persson, L. von Sydow, Pricing american options using a space-time adaptive finite difference method, *Math. Comput. Simulat.*, **80** (2010), 1922–1935. https://doi.org/10.1016/j.matcom.2010.02.008
7. J. C. Ndogmo, D. B. Ntwiga, High-order accurate implicit methods for barrier option pricing, *Appl. Math. Comput.*, **218** (2011), 2210–2224. https://doi.org/10.1016/j.amc.2011.07.037
8. P. P. Boyle, Y. Tian, An explicit finite difference approach to the pricing of barrier options, *Appl. Math. Financ.*, **5** (1998), 17–43. https://doi.org/10.1353/imag.2003.0128

9. J. Jeon, S. Y. Choi, J. H. Yoon, Analytic valuation of european continuous-installment barrier options, *J. Comput. Appl. Math.*, **363** (2020), 392–412. https://doi.org/10.1016/j.cam.2019.06.021
10. Y. C. Hong, S. Lee, T. G. Li, Numerical method of pricing discretely monitored barrier option, *J. Comput. Appl. Math.*, **278** (2015), 149–161. https://doi.org/10.1016/j.cam.2014.08.022
11. J. Lyu, E. Park, S. Kim, W. Lee, C. Lee, S. Yoon, et al., Optimal non-uniform finite difference grids for the Black–Scholes equations, *Math. Comput. Simul.*, **182** (2021), 690–704. https://doi.org/10.1016/j.matcom.2020.12.002
12. J. F. Yang, G. L. Li, On sparse grid interpolation for american option pricing with multiple underlying assets, *J. Comput. Appl. Math.*, **464** (2025), 116544. https://doi.org/10.1016/j.cam.2025.116544
13. M. Briani, L. Caramellino, A. Zanette, A hybrid tree/finite-difference approach for Heston–Hull–White-type models, *J. Comput. Financ.*, **21** (2017), 1–45.
14. S. O'Sullivan, C. O'Sullivan, On the acceleration of explicit finite difference methods for option pricing, *Quant. Financ.*, **11** (2011), 1177–1191. https://doi.org/10.1080/14697680903055570
15. D. S. Attipoe, A. Tambue, Convergence of the mimetic finite difference and fitted mimetic finite difference method for options pricing, *Appl. Math. Comput.*, **401** (2021). https://doi.org/10.1016/j.amc.2021.126060
16. P. Roul, V. M. K. P. Goura, A compact finite difference scheme for fractional Black-Scholes option pricing model, *Appl. Numer. Math.*, **166** (2021), 40–60. https://doi.org/10.1016/j.apnum.2021.03.017
17. H. Lim, S. Lee, G. Kim, Efficient pricing of bermudan options using recombining quadratures, *J. Comput. Appl. Math.*, **271** (2014), 195–205. https://doi.org/10.1016/j.cam.2014.04.007
18. M. Huang, G. Luo, A simple and efficient numerical method for pricing discretely monitored early-exercise options, *Appl. Math. Comput.*, **422** (2022). https://doi.org/10.1016/j.amc.2022.126985
19. C. Lee, J. Lyu, E. Park, W. Lee, S. Kim, D. Jeong, et al., Super-fast computation for the three-asset equity-linked securities using the finite difference method, *Mathematics*, **8** (2020), 307. https://doi.org/10.12946/rg28/307-309
20. J. P. Fouque, C. H. Han, Y. Z. Lai, *Variance reduction for MC/QMC methods to evaluate option prices*, In: Recent Advances in Financial Engineering, World Scientific, Singapore, 2009, 27–48. https://doi.org/10.1142/7301
21. P. Jäckel, *Monte Carlo methods in finance*, John Wiley & Sons, Chichester, UK, 2002.
22. C. Joy, P. P. Boyle, K. S. Tan, Quasi-Monte Carlo methods in numerical finance, *Manag. Sci.*, **42** (1996), 926–938. https://doi.org/10.1287/mnsc.42.6.926
23. M. H. Shi, Y. Y. Huang, X. F. Li, Y. L. Lei, J. J. Du, Monte Carlo method in stock trading research based on accelerated diffusion theory with jumps, *Physica A*, **672** (2025). https://doi.org/10.1016/j.physa.2025.130667
24. V. D. Doan, A. Gaikwad, M. Bossy, F. Baude, I. Stokes-Rees, Parallel pricing algorithms for multi-dimensional bermudan/american options using Monte Carlo methods, *Math. Comput. Simulat.*, **81** (2010), 568–577. https://doi.org/10.1016/j.matcom.2010.08.005
25. Z. J. He, X. Q. Wang, An integrated quasi-Monte Carlo method for handling high dimensional problems with discontinuities in financial engineering, *Comput. Econ.*, **57** (2020), 693–718. https://doi.org/10.1007/s10614-020-09976-2

26. H. W. Teng, M. H. Kang, On accelerating Monte Carlo integration using orthogonal projections, *Methodol. Comput. Appl.*, **24** (2021), 1143–1168. https://doi.org/10.1007/s11009-021-09893-3
27. A. D. Andricopoulos, M. Widdicks, P. W. Duck, D. P. Newton, Universal option valuation using quadrature methods, *J. Financ. Econ.*, **67** (2003), 447–471. https://doi.org/10.1016/S0304-405X(02)00257-X
28. D. S. Attipoe, A. Tambue, Novel numerical techniques based on mimetic finite difference method for pricing two dimensional options, *Results Appl. Math.*, **13** (2022). https://doi.org/10.1016/j.rinam.2021.100229
29. S. Kozpınar, M. Uzunca, B. Karasözen, Pricing european and american options under Heston model using discontinuous galerkin finite elements, *Math. Comput. Simulat.*, **177** (2020), 568–587. https://doi.org/10.1016/j.matcom.2020.05.022
30. Y. M. Lu, Y. D. Lyuu, Very fast algorithms for implied barriers and moving-barrier options pricing, *Math. Comput. Simulat.*, **205** (2023), 251–271. https://doi.org/10.1016/j.matcom.2022.09.018
31. S. E. Fadugba, Homotopy analysis method and its applications in the valuation of european call options with time-fractional Black-Scholes equation, *Chaos Soliton. Fract.*, **141** (2020). https://doi.org/10.1016/j.chaos.2020.110351
32. S. M. Nuugulu, F. Gideon, K. C. Patidar, A robust numerical scheme for a time-fractional Black-Scholes partial differential equation describing stock exchange dynamics, *Chaos Soliton. Fract.*, **145** (2021). https://doi.org/10.1016/j.chaos.2021.110753
33. J. R. Liang, J. Wang, W. J. Zhang, W. Y. Qiu, F. Y. Ren, Option pricing of a bi-fractional Black–Merton–Scholes model with the hurst exponent h in [1/2, 1], *Appl. Math. Lett.*, **23** (2010), 859–863. https://doi.org/10.1016/j.aml.2010.03.022
34. M. Rezaei, A. R. Yazdanian, A. Ashrafi, S. M. Mahmoudi, Numerical pricing based on fractional Black–Scholes equation with time-dependent parameters under the cev model: Double barrier options, *Comput. Math. Appl.*, **90** (2021), 104–111. https://doi.org/10.1016/j.camwa.2021.02.021
35. J. H. Chen, X. F. Li, Y. Z. Shao, Numerical analysis of fractional order Black–Scholes option pricing model with band equation method, *J. Comput. Appl. Math.*, **451** (2024). https://doi.org/10.1016/j.cam.2024.115998
36. J. Cho, Y. Kim, S. Lee, An accurate and stable numerical method for option hedge parameters, *Appl. Math. Comput.*, **430** (2022). https://doi.org/10.1016/j.amc.2022.127276
37. J. Cho, D. Yang, Y. Kim, S. Lee, An operator splitting method for multi-asset options with the Feynman-Kac formula, *Comput. Math. Appl.*, **135** (2023), 93–101. https://doi.org/10.1016/j.camwa.2023.01.019
38. M. N. Özişik, H. R. B. Orlande, M. J. Colaço, R. M. Cotta, *Finite difference methods in heat transfer*, CRC Press, 2 Eds., 2017. https://doi.org/10.1201/9781315121475
39. P. Glasserman, *Monte Carlo methods in financial engineering*, Springer, New York, 2003.
40. E. G. Haug, *The complete guide to option pricing formulas*, McGraw-Hill, New York, 2 Eds., 2007.

© 2025 the Author(s), licensee AIMS Press. This is an open access article distributed under the terms of the Creative Commons Attribution License (https://creativecommons.org/licenses/by/4.0)